

# A CONSTITUTIVE MODEL FOR THE SUPERPLASTIC MATERIAL ALNOVI-1 INCLUDING LEAK RISK INFORMATION

Corijn H.C. Snippe<sup>1</sup>, Timo Meinders<sup>2</sup>

<sup>1</sup>National Institute for Nuclear and High-Energy Physics (Nikhef)  
Kruislaan 409, 1098 SJ Amsterdam, The Netherlands

<sup>2</sup>University of Twente

Mechanics of Forming Processes, Department of Mechanical Engineering  
Drienerlolaan 5, 7522 NB Enschede, The Netherlands

## ABSTRACT

For some applications, it is important that a formed sheet of material is completely gas tight, therefore it is beneficial to be able to predict whether a formed sheet will be leak tight for gases or not. Superplastic materials show the ability to attain very high plastic strains before failure. These strains can only be reached within a small range of temperature and strain rate. In the case of the aluminium alloy ALNOVI-1 by Furukawa Sky Aluminium, the optimum superplastic behaviour is found at 520 °C and at strain rates roughly between  $10^{-4}$  to  $10^{-2}$  s<sup>-1</sup>. Under these conditions, the mechanical behaviour of the material is highly strain rate dependent. This article describes a proposal for the constitutive model of ALNOVI-1, as can be incorporated into an FE code (like a user-defined material UMAT in ABAQUS), in which the leak risk can be implemented, as function of the cavity volume fraction. This will be done in a phenomenological way, using the results of uniaxial tensile and biaxial bulge experiments.

**Keywords:** Superplasticity, ALNOVI-1, constitutive model

## 1. SUPERPLASTICITY

Superplastic materials show a very high sensitivity in mechanical properties with respect to the strain rate, especially the flow stress is determined highly by this quantity.

### 1.1 Initial flow stress

Since the strain rate is the dominating factor, a very simple expression for the flow stress  $\sigma_f$  is sometimes used in calculations involving superplastic material behaviour. This equation involves the influence of the strain rate by an exponent  $m$  only, which is the *strain rate sensitivity*

$$\sigma_f = k \dot{\epsilon}^m \quad (1)$$

and in which  $k$  is a material constant. When this stress is plotted against the strain rate in a log-log diagram, this results in a straight line with slope  $m$ . However, in reality, it appears from experiments that this line is not straight, but shows a sigmoidal curve, as can be seen in Figure 1. The curve is divided into three areas as shown in the figure.

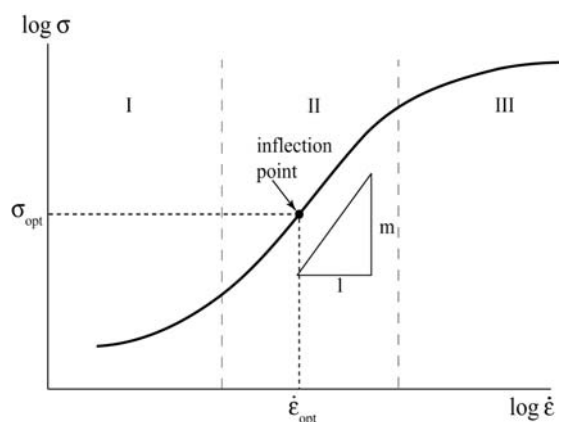


Figure 1. Initial flow stress of a superplastic material, showing a sigmoidal curve.

The point where the highest slope can be found is called the *inflection point* of the curve, and is situated in the relatively narrow area II. Hence,  $m$  is not constant but dependent on the strain rate (see Figure 2).

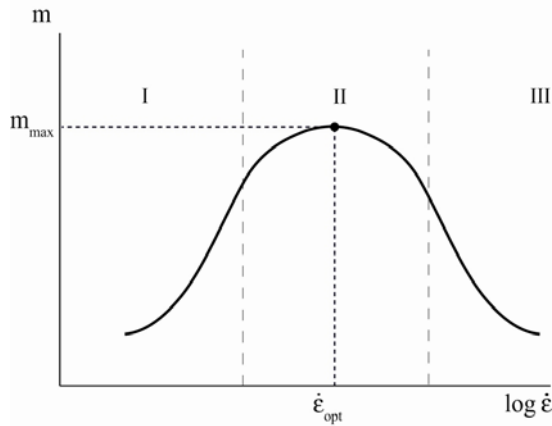


Figure 2. Strain rate sensitivity  $m$  as function of the strain rate.

In fact,  $m$  can be considered constant over a narrow range of strain rates, so Equation (1) is only valid within this very small range.

## 1.2 Strain hardening

Most materials show an increasing flow stress with an increasing plastic strain. This is also the case with superplastic materials, but the hardening mechanism is thought to be different from the strain hardening mechanism of conventional materials: they follow the Hall-Petch effect, which proposes a relationship between grain size and flow stress, showing lower flow stresses at higher grain sizes. Since in superplasticity it is believed that strain hardening is caused by grain growth, it seems straightforward that a relationship is constructed between these two quantities. At elevated temperatures, high enough for superplastic material behaviour, the grain boundaries are weaker than the grains themselves, so the Hall-Petch effect is not applicable in that case. Superplastic alloys have generally a good resistance against grain growth, which is a result of the alloying elements.

Two types of grain growth work independently from each other: static and dynamic grain growth. Static grain growth is caused by the elevated temperature, dynamic grain

growth by the deformation. Both types of grain growth are clearly visible from the grain size evolution law described in [1]

$$\dot{d} = M\sigma_{\text{surf}}d^{-r_0} + \alpha\dot{\epsilon}d^{-r_1} \quad (2)$$

in which  $r_0$ ,  $r_1$  and  $\alpha$  are constants,  $M$  is the grain boundary mobility and  $\sigma_{\text{surf}}$  is the grain boundary energy density. If the first part of this equation (static grain growth) is ignored, since the second term is the dominating factor, this equation can be simplified such that the grain size is only influenced by the strain and the initial grain size, and becomes independent of the strain rate. An expression for the flow stress as function of the strain can be set up as

$$\sigma_{f,h} = \sigma_{f,ini} + \Delta\sigma \left[ 1 - \exp\left(-\frac{\epsilon}{\epsilon_0}\right) \right] \quad (3)$$

where  $\sigma_{f,h}$  is the flow stress,  $\sigma_{f,ini}$  is the initial flow stress. This conforms to Voce hardening [2], a hardening model where the stress goes asymptotically to a *saturation stress*  $\Delta\sigma$ . The parameter  $\epsilon_0$  determines the rate of approaching the saturation stress.

## 1.3 Strain softening

Cavity growth is the main reason for the macromechanical softening of a superplastic material. Several studies describe the behaviour of cavities in (superplastic) materials. The best known is Gurson's porous metal plasticity model (Gurson, 1977), based on a spherical void in a unit cell. The void growth is determined as function of the rate-of-deformation tensor  $\mathbf{D}$ . This model takes into account that the voids already exist in the initial configuration and no void nucleation takes place. Needleman (1978, 1980) developed a model for the nucleation of voids, which can be considered stress- or strain-driven. The advantage of the first one is that a hydrostatic stress can be accounted for [3]:

$$\dot{\xi} = (1 - \xi) \text{tr}(\mathbf{D}) + A\dot{\sigma}_y + B\dot{\Sigma}_h \quad (4)$$

in which  $\zeta$  is the void volume fraction,  $\sigma_y$  is the yield stress of the matrix material and  $\Sigma_h$  is the average hydrostatic stress in the material.  $A$  and  $B$  are constants. An expression for the macroscopic flow stress is [4]

$$\sigma_f = \sigma_m (1 - n_1 \zeta^{n_2})^{n_3} \quad (5)$$

where  $\sigma_f$  is the macromechanical flow stress,  $\sigma_m$  is the stress in the matrix material and  $n_1$ ,  $n_2$  and  $n_3$  are adjusting parameters. These parameters have to be determined with uniaxial tensile experiments. Cavity growth eventually leads to the coalescence of these cavities, which is the onset of fracture. In case of gas leakage through a formed sheet, the material can be considered failed if enough cavities can interlink to provide through-thickness channels.

#### 1.4 Backpressure

The application of a hydrostatic backpressure on the sheet inhibits the formation and growth of cavities. This means that the coalescence stage in the cavitation behaviour is postponed. Khaleel et al [4] shows the behaviour of the material ALNOVI-1 in case a backpressure during forming is applied. An increase in maximum cup height in free bulging experiments was observed.

## 2. UNIAXIAL EXPERIMENTS

ALNOVI-1 is a material, based on the aluminium alloy AA5083. This material contains besides about 4% of Magnesium, also 0.8% of Manganese, of which the latter addition slows down the process of static grain growth. In order to obtain a set of uniaxial stress-strain curves for ALNOVI-1 at its optimal superplastic temperature, tensile experiments have been performed on this material. First, the setup is described, (specimen geometry and testing procedure). Then the results are presented, where also the method of determining the stress-strain curves is worked out.

Two kinds of tests were performed. Firstly, a series of destructive tests (test I) were performed, where the tensile specimens were loaded until fracture. In the second test se-

ries (test II), the specimens were loaded until a prescribed value of the elongation. These tests are used to study the cavity volume fraction at different values for the plastic strain.

#### 2.1 Uniaxial experiments: setup

The tensile tests are executed on samples of which the geometry is shown in Figure 3.

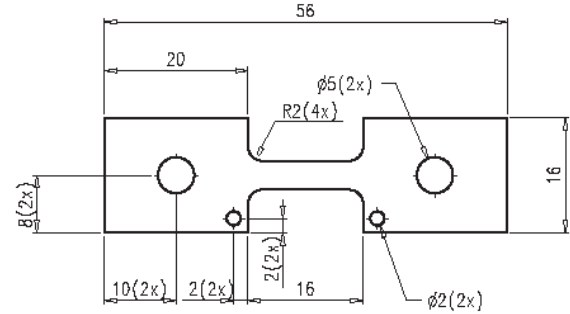


Figure 3. Specimen geometry for the tensile experiments.

The tensile direction of the samples is chosen to lie parallel or perpendicular to the rolling direction, or at an angle of  $45^\circ$  to the rolling direction. A sample was connected freely by its two holes to the two tensile arms of the testing machine. The two small holes were used to attach thermocouples to make sure that the temperature stays at the optimal superplastic temperature (which was found to be at  $520^\circ\text{C}$ ). A tunnel furnace heated the specimen; when the thermocouples read the correct temperature, the test started with an extra delay of five minutes. The specimen was then drawn at a constant cross-head velocity. The output of the tester was the tensile force vs. time, which can be interpreted as tensile force vs. displacement, since the velocity is known.

#### 2.2 Uniaxial experiments: results, test I

The destructive tests in which the specimens were all loaded until fracture, resulted in force-displacement curves for a set of six different cross-head velocities. The first observation is that the forces are very low compared to results usually obtained in tensile tests on aluminium specimens. The force-displacement data were translated into

a set of stress-strain curves by an iterative procedure between the experimental force-displacement data and an FE simulation of the tensile experiment. In these simulations, besides the tensile force, also some dimensional features were checked, for instance the deformation of the connection holes. This procedure resulted in the set of stress-strain curves shown in Figure 4.

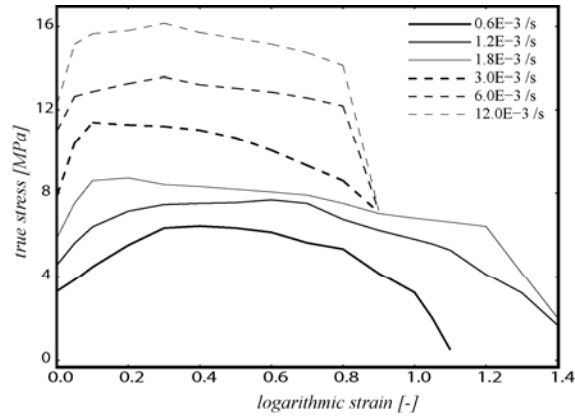


Figure 4. ALNOVI-1 stress-strain curves at six different strain rates.

The initial flow stresses (at zero plastic strain) for the different strain rates are plotted in Figure 5, the points are connected by straight lines for visualisation reasons.

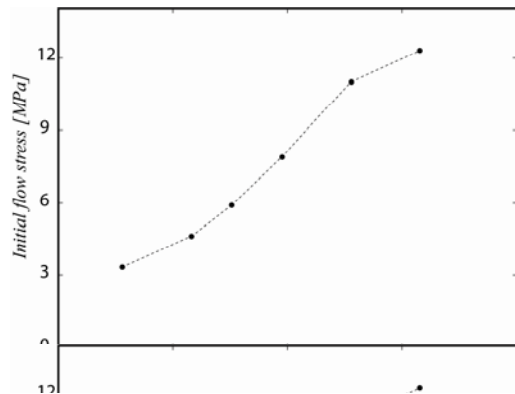


Figure 5. Initial flow stress [MPa] as function of the strain rate [ $s^{-1}$ ].

Although this is a plot with only six points, a sigmoidal shape is visible. The maximum strain rate sensitivity  $m_{\max}$  is 0.61, which is a normal value for superplastic materials.

### 2.3 Uniaxial experiments: results, test II

The second series of experiments deal with the non-destructive tests, in which the ten-

sile specimens are loaded until a prescribed value of the displacement.

Cavity volume fractions can be determined by polishing the drawn specimens and observing them under a light microscope. From the specimens belonging to three strain rates (from the simulations it followed that because of the geometry, the strain rate during the test was close to constant), some specimens were observed. The results from these observations are shown in Figure 6.

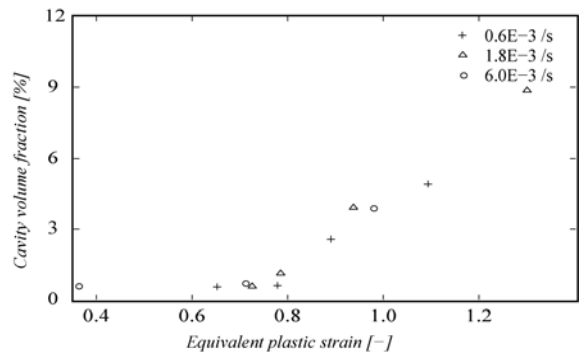


Figure 6. Cavity volume fractions as function of the equivalent plastic strain.

It seems that the cavity volume fractions are more influenced by the equivalent plastic strain than by the strain rate.

### 3. BIAXIAL EXPERIMENTS

Biaxial tests are performed to obtain insight into the following points:

- gas (i.e. Helium) leak through the formed sheet as function of the cavity volume fraction;
- influence of a backpressure on the formability and the leak rate of a formed sheet.

The stress-strain data as constructed from the uniaxial tensile experiments, were used as input for the FE calculations in which free bulging experiments are simulated. These simulations have to predict the pressure applied on a sheet in time. A user subroutine, coupled to the FE code reads the plastic strain rates every increment, which are used to calculate the pressure in the next time increment. This subroutine controls the pressure in such a way that a target

strain rate will not be exceeded in the model.

### 3.1 Biaxial experiments: setup

Three target strain rates are used to calculate the pressure-time curves for four different initial sheet thicknesses. Figure 7 shows the calculated pressure-time curves for an initial sheet thickness of 1.0 mm for these three target strain rates.

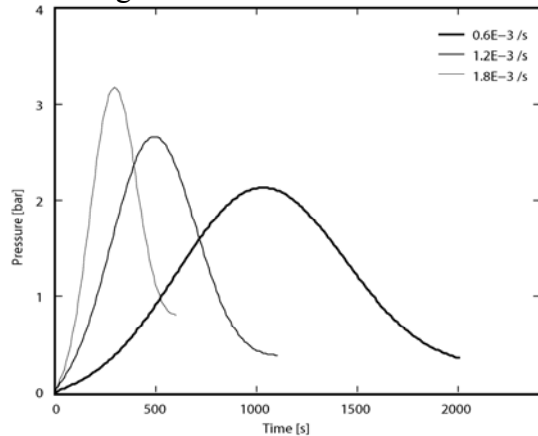


Figure 7. Pressure-time curves to be used in the free bulging experiments.

These curves were used in an experimental setup, which is described in the next subsection. The results of these experiments are discussed in Sections 3.2 and 3.3.

A sheet is positioned inside the setup, after which the temperature is raised until 520 °C. The sheet is clamped after this temperature increase in order to prevent internal stresses due to thermal expansion. A hydrostatic pressure (if necessary) is then applied, after which the forming pressure will force the bulging of the sheet into the cylindrical die. Three values for the hydrostatic pressure were used: 14, 20 and 30 bar.

### 3.2 Biaxial experiments: results

In this section, the results of the 1.0 mm thick sheets are presented. All sheets were pressed until a prescribed time step or until the formed sheet leaks gas through the sheet (which is directly visible because the forming pressure immediately drops in that case). The results are categorised according to target strain rate and to hydrostatic pressure.

#### 3.2.1 Maximum cup height

In Table 1, the maximum cup heights are presented for all three target strain rates, and in the cases of zero and 14 bar backpressure.

Table 1. Maximum cup heights (in mm), 0 and 14 bar backpressure, at three target strain rates.

	$0.6 \cdot 10^{-3} [s^{-1}]$	$1.2 \cdot 10^{-3} [s^{-1}]$	$1.8 \cdot 10^{-3} [s^{-1}]$
0	43.20	41.40	44.61
14	45.33	45.10	48.26

From these results, the statement in Section 1.4 confirms that with backpressure, maximum cup heights are larger than without a backpressure. There is no clear relationship between the target strain rate and the maximum cup height. Table 2 shows that with increasing backpressure, the maximum cup height can be increased further.

Table 2. Maximum cup heights, dependent on the applied backpressure.

backpressure [bar]	0	14	20	30
maximum cup height [mm]	44.61	48.26	48.44	51.32

A picture of the cup reaching a height of 51.32 mm is shown in Figure 8.

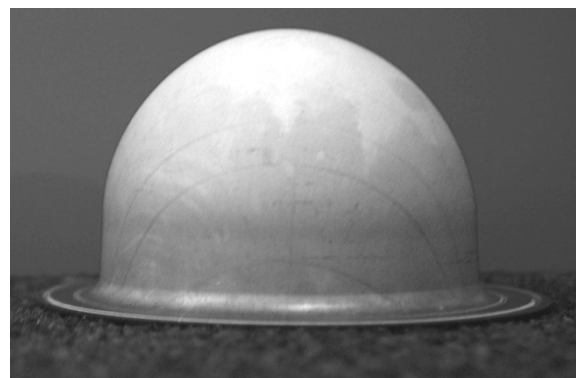


Figure 8. Cup which reached the record height of 51.32 mm.

#### 3.2.2 Top thickness

Besides the cup height, also the sheet thickness in the top of the bulge is measured. Figure 9 shows the dependence of this top

thickness with respect to the bulge height, for the three target strain rates.

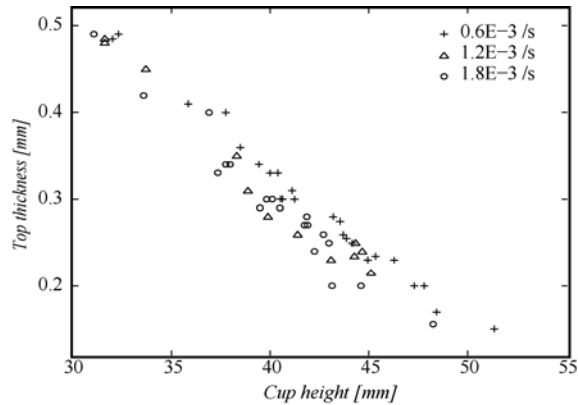


Figure 9. Top thickness as function of the cup height.

It is visible, that the lowest target strain rate deviates from the other two, in such a way that these cups are thicker in the top at the same bulge height. This means that in case of the lowest strain rate, the material flows more from the sides to the top part of the cup. This has also been verified by carrying out thickness measurements on the sides, also stretches have been measured by applying a grid onto the undeformed sheet.

### 3.2.3 Leak rate

Part of the cups already failed during the test, which means that fracture occurred in the top part of the cup. But before fracture arises, the cavities will coalesce and create channels through the thickness of the sheet. All the cups which did not fracture in the bulging experiment were leak tested. The space at the outer side of the cup in the leak test setup was made vacuum, the inner side was filled with Helium at atmospheric pressure. The leak rate is measured by the tester, expressed in  $[\text{mbar} \cdot \text{l} / \text{s}]$ , this is a general accepted unit for leak measurements. Figure 10 shows a the leak rate of the cups as a function of the cup height.

The most interesting area in this graph are the four data points at the bottom right part, which represent the cups with a large height and a very good leak tightness. These cups were all formed while a backpressure of 30 bar was applied.

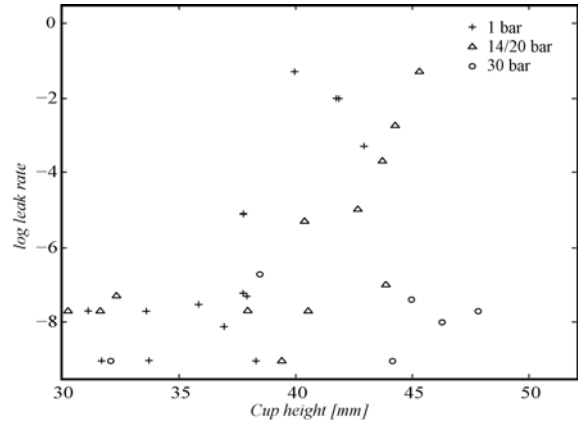


Figure 10. Leak rate as function of the cup height.

Also the cups formed with a backpressure of 14 or 20 bar have a better leak tightness than the cups formed without a backpressure. It is obvious to conclude that the improved leak tightness at higher backpressures is because cavity growth is inhibited by this backpressure, and cavity coalescence is postponed.

## 4. MATERIAL MODEL

The initial flow stress, as dependent on the strain rate, is described by an equation for a sigmoidal curve. The parameters to shape this curve can be derived from the uniaxial tensile experiments only. The same holds for the strain hardening and softening parts. The biaxial results are used to find relations between equivalent plastic strain, cavity volume fraction and leak rate.

### 4.1 Initial flow stress

The data shown in Figure 5 can be fitted to a sigmoidal curve, by using four parameters  $a$ ,  $b$ ,  $c$  and  $d$  to adjust the standard sigmoidal curve equation to

$$\log \sigma_{f,ini} = \frac{1}{a + b \exp(c \log \dot{\epsilon})} + d \quad (6)$$

The best fit of these parameters are shown in Table 3 (units of stress are in  $\text{N}/\text{m}^2$ ).

Table 3. Best fit for  $a$ ,  $b$ ,  $c$  and  $d$

$a$	$b$	$c$	$d$
1.4446	$3.5633 \cdot 10^{-5}$	-3.8901	6.4332

## 4.2 Strain hardening

Strain hardening is caused by grain growth in the material. However, the grain size itself is not measured in this material, so the hardening part will be carried out by fitting the results to an equation following the Voce hardening model. From the stress-strain relationships as shown in Figure 4, the saturation stress  $\Delta\sigma$  (see Equation (3)) can be interpreted as the maximum flow stress minus the initial flow stress. The results of this subtraction are presented in Table 4. The mean saturation stress is about 3.1 MPa, the largest deviations occur at strain rates where the material already loses some of its superplastic behaviour.

Table 4. Saturation stress  $\Delta\sigma$  as function of the strain rate.

Strain rate [ $\times 10^{-3} \text{ s}^{-1}$ ]	Saturation stress [MPa]
0.6	3.15
1.2	3.08
1.8	2.82
3.0	3.31
6.0	2.59
12.0	3.85

So, if the material is considered to behave superplastically, a constant saturation stress will be assumed, being the mean stress of the first four entries in the table, so  $\Delta\sigma = 3.1$  MPa.

The parameter  $\varepsilon_0$  is the strain at which a hardening stress of  $0.632 \cdot \Delta\sigma$  is reached. From the results it follows that this strain decreases with increasing strain rate, an approximation is found

$$\varepsilon_0 \dot{\varepsilon} = 1.2 \times 10^{-4} \quad [\text{s}^{-1}] \quad (7)$$

## 4.3 Strain softening

Just as the initial flow stress  $\sigma_{f,ini}$  and the stress due to hardening  $\sigma_{f,h}$ , the softening can also be fitted directly to a predefined curve. But since the cavity volume fraction is important here, because it influences the leak rate, the softening stress is made de-

pendent on the cavity volume fraction, as in Equation (5).

The results shown in Figure 6 can be interpreted as a bilinear relationship, where above a threshold strain  $\varepsilon_{tr}$ , the cavity volume fraction is

$$\begin{aligned} \xi &= 0.83\varepsilon & , \varepsilon \leq 0.74 \\ \xi &= 14.1\varepsilon - 9.8 & , \varepsilon > 0.74 \end{aligned} \quad (8)$$

The flow stress can be determined by determining the parameters  $n_1$ ,  $n_2$  and  $n_3$  from Equation (5). Table 5 shows the best fit for these parameters.

Table 5. Best fit for  $n_1$ ,  $n_2$  and  $n_3$ .

$n_1$	$n_2$	$n_3$
0.0672	0.946	1.272

## 4.4 Backpressure

From literature and the experiments carried out here, it follows that a backpressure inhibits the cavity growth, this means that especially the softening part of the stress-strain curves is influenced.

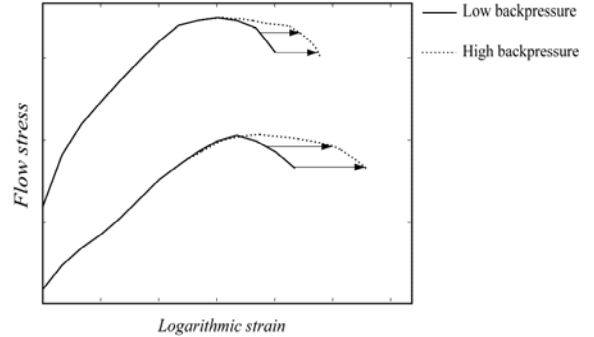


Figure 11. ‘Stretching’ of the stress-strain curves to represent a hydrostatic pressure.

In one dimension, the softening part of the stress-strain curves can be thought of as stretched in the direction of the strain axis, see Figure 11.

## 4.5 Implementation into UMAT

The results can be implemented in a user-defined material model. Besides the uniaxial properties, also a yield criterion has to be added. It is assumed that the flow behaviour conforms to a Hosford type, with  $m = 8$  (where in case of von Mises flow,  $m = 2$ ):

$$\left( |\sigma_1 - \sigma_2|^m + |\sigma_2 - \sigma_3|^m + |\sigma_3 - \sigma_1|^m \right)^{1/m} = 2\sigma_f \quad (9)$$

Since this yield criterion is defined in the direction of the principal axes, these directions have to be calculated in the material model.

Also, a return-mapping procedure is necessary. Here it is chosen to use a general algorithm which projects the elastic trial stress perpendicularly onto the yield surface, by using an implicit Newton algorithm to update the plastic strain components, as dependent on the equivalent plastic strain rate.

## 5. VERIFICATION

The model, as proposed in the previous chapter, is used to calculate the forces in the simulated uniaxial tensile tests. The results are shown in Figure 12, which shows that the simulation results are in good agreement with the experimental results.

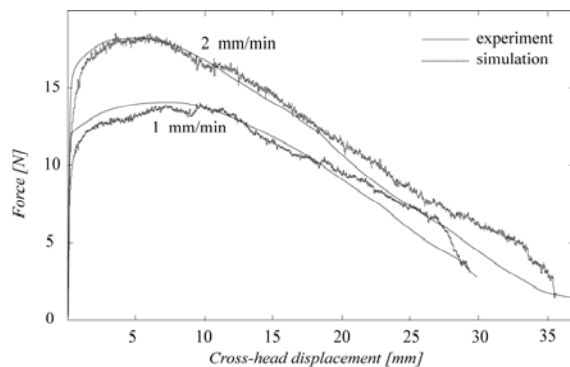


Figure 12. Force-displacement curves: simulation vs. experiment, for two cross-head velocities.

## 6. CONCLUSIONS

From the uniaxial and biaxial experiments, some typical material behaviour can be observed. Firstly, the material is highly strain rate dependent at the optimal superplastic temperature, the stress-strain curves lie far apart from each other. Secondly, the strain rate in the material determines the top thickness of a formed cup, a lower strain rate results in a more evenly distributed sheet thickness in the whole cup. Thirdly, the application of a backpressure during

forming operations has a positive influence on the leak tightness of a formed cup.

Future work includes carrying out biaxial experiments on sheets with other sheet thicknesses; studying the effect of friction by using a different die; verification of the user-defined material model; studying cavity volume fractions of the formed cups.

## LIST OF REFERENCES

1. Lin J., Dean T.A., "Modelling of microstructure evolution in hot forming using unified constitutive equations", *Jnl. of Mat. Processing*, vol. 167, 2005, pp. 354-362.
2. Huétink J., Brekelmans W.A.M., Peerlings R.H.J., van den Boogaard A.H., Meinders V.T., Geijselaers H.J.M., "Mechanics of Forming Processes", Graduate Course EM School, Ch12, University of Twente, 2003.
3. Peerlings R., "Plasticity of Porous Materials", Graduate Course Micromechanics, University of Technology Eindhoven, 2004.
4. Khaleel M., Zbib H., Nyberg E., "Constitutive modeling of deformation and damage in superplastic materials", *Intl. Jnl. of Plasticity*, vol. 17, 2001, pp. 277-296.
5. Syn C.K., O'Brien M.J., Lesuer D.R., Sherby O.D., "An Analysis of Gas Pressure Forming of Superplastic AL 5083 Alloy", Lawrence Livermore National Laboratory, UCRL-JC-135190, 2001.